JOURNAL OF SOLID STATE CHEMISTRY 108, 253–259 (1994)

Low-Dimensional and Extended Metal—Metal Bonded Networks in Transition Metal Compounds: $Ba_2Nb_5O_9$, $Ba_{2-x}Y_xNb_5O_9$

Hea-Ri Lee, Sung-Jin Kim,*,[1] In-Sang Yang,† and Jin-Ho Choy‡

*Departments of *Chemistry and †Physics, Ewha Women's University, Seoul, Korea; and ‡Department of Chemistry, Seoul National University, Seoul, Korea*

Received February 23, 1993; in revised form May 19, 1993; accepted May 21, 1993

The crystal structure, oxidation state, electronic properties of unusual niobates which contain niobium clusters condensed low dimensionally, were investigated by X-ray diffraction, X-ray photoelectron spectroscopy (XPS), electrical resistivity measurements, and Raman spectroscopy. The results of XPS experiment indicate that there are three niobium oxidation states (Nb^{4+}, Nb^{3+}, Nb^{2+}) in $Ba_2Nb_5O_9$ and these oxidation states are expected to be stable considering their atomic coordinates. Pure $BaNbO_3$ phase was synthesized and its niobium oxidation state was examined in order to compare with those of niobium in $Ba_2Nb_5O_9$. Electrical resistivity measurements on $Ba_2Nb_5O_9$ show negative $d\rho/dT$ behavior between 160 K and 600 K. Similar behavior was observed in yttrium substituted niobates, $Ba_{2-x}Y_xNb_5O_9$. The possibility of relationship between low dimensionality and anomalous properties of these niobates is discussed. © 1994 Academic Press, Inc.

1. INTRODUCTION

Since Svensson and co-workers found $Ba_2Nb_5O_9$, there have been growing interests in similar new reduced niobates (1–3). Michelson *et al.* have found more niobate phases ($Sr_2Nb_5O_9$, $K_2Nb_5O_9$, and KNb_3O_5) and reported anomalous electronic properties in $Ba_2Nb_5O_9$ (4). These niobates commonly contain Nb_6O_{12} and NbO_6 octahedral clusters and their structures can be described as an intergrowth of perovskite-like Ba_2NbO_4 and NbO-like Nb_4O_5 layers. Three-dimensional condensation of Nb_6O_{12} octahedral clusters (the octahedral Nb_6 clusters are edge-capped by twelve oxygens to make Nb_6O_{12} clusters, and Nb_6 clusters are condensed by sharing corners) occurs in NbO and that of NbO_6 clusters (by sharing corners) occurs in $BaNbO_3$. In $Ba_2Nb_5O_9$, three-dimensional networks of Nb_6O_{12} and NbO_6 octahedral clusters are modified to become two-dimensional layers, and these two layers are intergrown in ordered way as shown in Fig. 5.

Even though the cubic $BaNbO_3$ phase was first reported in 1955 (5), the exact barium occupancy is not clearly known. Kreiser and Ward reported barium deficient perovskite (6) and recently Svensson reported perovskite with full barium occupancy (7). However, it was known that strontium occupancy ranges from 0.7 to 0.95, and unit cell parameters obey the Vegard law in Sr_xNbO_3 perovskite. We synthesized a pure $BaNbO_3$ phase and compared the niobium character of this material with that of $Ba_2Nb_5O_9$. Results of our X-ray photoelectron spectroscopic (XPS) experiments show that $Ba_2Nb_5O_9$ has three kinds of Nb atoms in different oxidation states, while all Nb atoms of $BaNbO_3$ are in one oxidation state (Nb^{4+}). We examined electrical resistivity of $Ba_2Nb_5O_9$ and $Ba_{2-x}Y_xNb_5O_9$, and found negative $d\rho/dT$ behavior between 160 and 600 K. The origin of these anomalous electronic properties is conjectured to be diffusion of charge carriers between layers (8).

2. EXPERIMENTAL

Two reduced niobates, $Ba_2Nb_5O_9$ and $BaNbO_3$, were synthesized from fully oxidized niobium compound, $Ba_5Nb_4O_{15}$. To synthesize $Ba_2Nb_5O_9$ and $BaNbO_3$, stoichiometric amounts of Nb, Nb_2O_5, and $Ba_5Nb_4O_{15}$ were ground and pressed into pellets, then heated to 1050°C for 24 hr in an evacuated quartz tube. $Ba_5Nb_4O_{15}$ was prepared from mixture of $BaCO_3$ and Nb_2O_5, and heated to 1100°C in air for 24 hr. $Ba_{2-x}Y_xNb_5O_9$ was synthesized from Y_2O_3, Nb, Nb_2O_5, and $Ba_5Nb_4O_{15}$ in a way similar to $Ba_2Nb_5O_9$.

X-ray measurements were taken at room temperature using a Siemens X-ray diffractometer and Cu$K\alpha$ radiation. Diffraction data were analyzed using Rietveld-type full-profile refinement technique (9), using a measuring step of 0.02° (in 2θ). A Rigaku X-ray diffractometer equipped with a Bühler sample chamber and temperature controller was used for studies at high temperatures (up to 900°C).

Electrical resistivities were measured using the four-probe method and sintered pellets. For low temperature (liquid nitrogen range) experiments, four wires were connected to the sample by indium contacts. For higher tem-

[1] To whom correspondence should be addressed.

0022-4596/94 $6.00

perature experiments (from room temperature to 900 K), tungsten wires were pressed to the sample directly and measurements were carried out under an argon atmosphere.

XPS experiments were carred out with a Surface Science instrument. Samples were mounted on an aluminum plate. Nonmonochromatic Al$K\alpha$ radiation was used as an excitation source ($h\nu$ = 1486.6 eV). During the measurement, the spectrometer was pumped to a residual pressure of about 10^{-9} Torr. The sample surfaces were mechanically scraped with a metal brush or sputtered by ion bombardment in order to expose fresh surfaces the 1s binding energy of carbon, 284.6 eV, was used as an internal standard.

Raman spectroscopy experiments were carried out with a Jobin Yvon U1000 double monochromator and the 514.5 nm line of Ar-ion laser in a back scattering geometry. Slit widths were 500 μm, corresponding to 4.6 cm^{-1} resolution. To obtain reproducible data, several crystals from the same pellet were measured during the experiments.

Tight-binding electronic structure calculation based upon the extended Hückel method (10) was performed for the $Ba_2Nb_5O_9$ system.

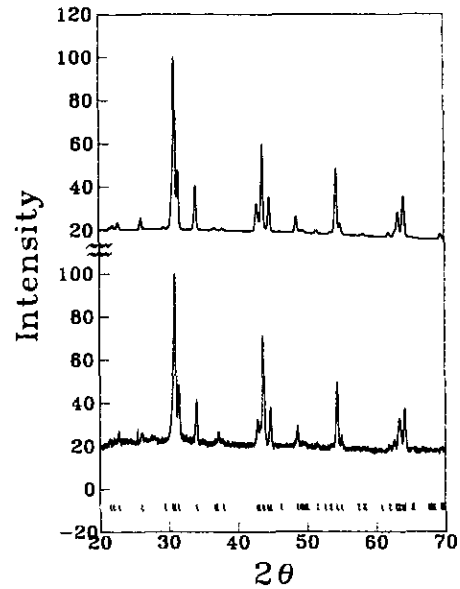

FIG. 1. Comparison of calculated (top) and observed (bottom) powder diffraction for $Ba_2Nb_5O_9$. Vertical strokes indicate calculated Bragg peak positions.

3. RESULTS AND DISCUSSION

The product with stoichiometry of $Ba_2Nb_5O_9$ was a homogeneous black powder. The powder X-ray diffraction pattern was refined with Rietveld-type full profile refinement. No extra peaks except the calculated pattern were found. The refined parameters used were scale factor, zero point, background parameters, cell parameters, atomic positions, and occupancies. No partial occupancies were indicated within standard deviations. (Fig. 1, Table 1)

The product with stoichiometry of $BaNbO_3$ was bright violet with metallic luster. The X-ray diffraction pattern did not have any impurity lines. Since we were interested in the oxidation state of Nb, we examined the occupancy of Ba sites using the Rietveld method and found the barium sites were fully occupied within standard deviation (fitting results are shown in Fig. 2). If the actual composition of this material were $Ba_{0.5}NbO_3$, the oxidation state of Nb could be +5. Direct current magnetic susceptibility measurement showed Pauli paramagnetism (7.2×10^{-7} emu/g), with absolute error of 20% at room temperature. A typical metallic behavior was observed with the resistivity of 2.8×10^{-3} ohm cm at 298 K. The maximum oxidation state of Nb is +5 with d^0 electron configuration, and fully oxidized niobates are insulators. However, the results of resistivity and susceptibility measurements confirm that this material is metallic. XPS experiments were carried out (Fig. 3) on a mechanically-scraped surface and the results are listed in Table 2. The experiments were performed also on an argon-sputtered surface. Two different methods to get clean surfaces were tried as above and the results were the same in this compound. The binding energy of Nb showed good agreement with NIST data for NbO_2 (11). The resistivity, susceptibility measurement, and XPS experiments suggest that the oxidation state of niobium in $BaNbO_3$ is +4 and d^1 electrons are delocalized.

To examine the oxidation state of niobium in various chemical bondings, XPS experiments were carried out (Fig. 4) for $Ba_2Nb_5O_9$. The surfaces of sample were prepared by the two methods as in $BaNbO_3$. Comparing two sets of data after the two different surface treatments, the data after argon sputtering showed multiple peaks

TABLE 1
Refined Parameters for $Ba_2Nb_5O_9$ in Tetragonal *P4/mmm* Unit Cell

Atom	Position (x, y, z)	Occupancy (%)
Ba	0, 0, 0.333(9)	100 (1)
Nb1	½, ½, ½	100 (1)
Nb2	½, ½, 0.1677(9)	100 (1)
Nb3	0, ½, 0	100 (1)
01	½, 0, ½	not refined
02	½, ½, 0.347(3)	not refined
03	½, 0, 0.2032(9)	not refined
04	0, 0, 0	not refined

Note. The figures within parentheses are the estimated standard deviations based on statistics. Refined results: R_{wp} = 6.61%. Unit cell: a = 4.1659(2) Å, c = 12.2256(9) Å.

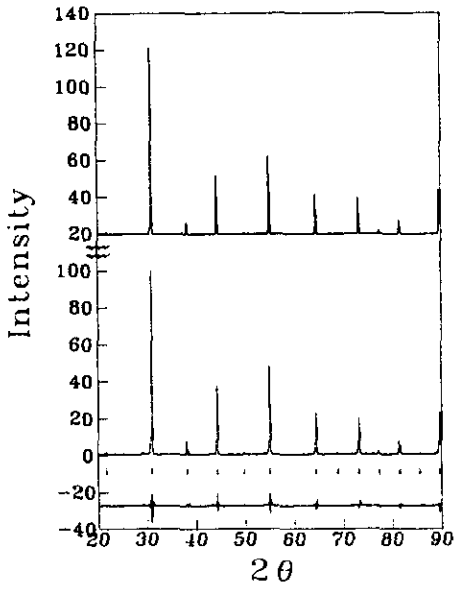

FIG. 2. Comparison of calculated (top) and observed (bottom) powder diffraction for $BaNbO_3$. Vertical strokes indicate calculated Bragg peak positions. No extra peaks are indicated. The unit cell parameter refined is 4.0939(3) Å in $Pm3m$. The resulting weighted profile R-value is 13%.

resolved clearly. XPS results from sputtered surfaces, especially surfaces of oxides, could have artifacts of reduction instead of a surface-cleaning effect. Since the change in oxidation state of niobium after ion sputtering was not observed in $BaNbO_3$, we may assume that the reduction is not serious for a qualitative analysis on similar

TABLE 2
Niobium $3d_{3/2}$. $3d_{5/2}$ Binding Energy of the $BaNbO_3$

Binding energy (eV)	State	Intensity (%)
209.1 ± 0.2	$d_{3/2}$ (Nb^{+4})	42
206.3 ± 0.2	$d_{5/2}$ (Nb^{+4})	58

niobate, $Ba_2Nb_5O_9$. The XPS results for niobium $3d_{3/2}$ and $3d_{5/2}$ binding energies are listed in Table 3. Peaks could be resolved into 3 pairs of $d_{3/2}$ and $d_{5/2}$. Crystallographically, there are two kinds of niobium, Nb(2) and Nb(3), in the Nb_4O_5 layers. Since Nb(1) has same NbO_6 coordination as in $BaNbO_3$ (Fig. 5), the oxidation state of Nb(1) could be assigned to +4, which corresponds to the peak at the highest binding energy in Fig. 4. The two peaks at lower binding energies could be assigned to Nb^{3+} for Nb(2) and Nb^{2+} for Nb(3), and these assignments seem to be reasonably based not only on charge balance but also on atomic coordinates around niobium atoms. Three different oxidation states are expected to be stable based on following reasons. There are six oxygens coordinated to Nb(1), the bond lengths of Nb(1)–O(1) and Nb(1)–O(2) are 2.08 and 1.54 Å, respectively (Fig. 6). Employing a crystal field approach, the energy levels of d orbitals are expected to be split into sublevels to stabilize the $d_{x^2-y^2}$, d_{xy} orbitals in a tetrahedrally contracted octahedral field and d^1 configuration is reasonably stable in Nb(1). There are five oxygen atoms coordinated around Nb(2). The bond lengths of four Nb(2)–O(3) and one Nb(2)–O(2) are 2.10 and 2.48 Å, respectively. The energy levels of d_{xz},

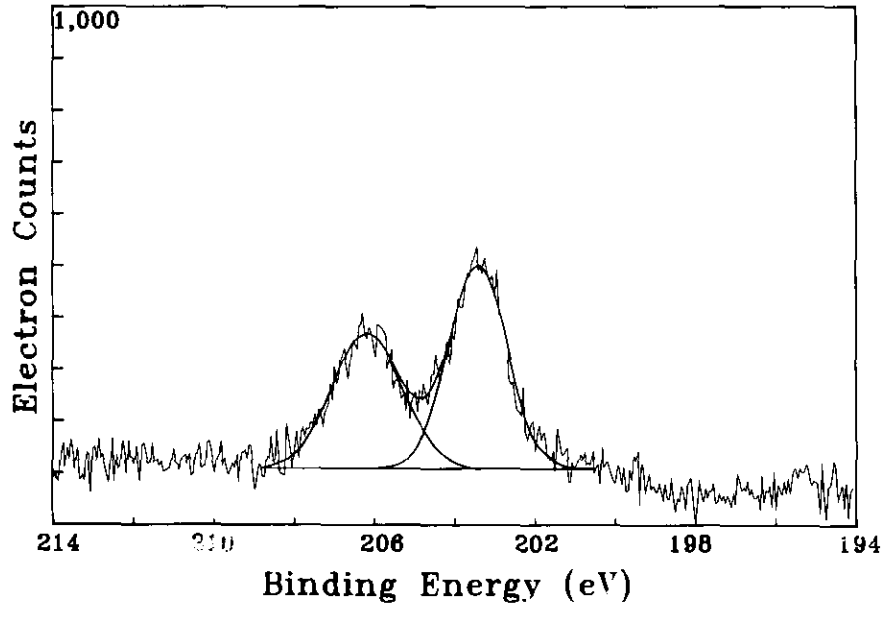

FIG. 3. Nb $3d$ core-level XPS spectrum for the $BaNbO_3$.

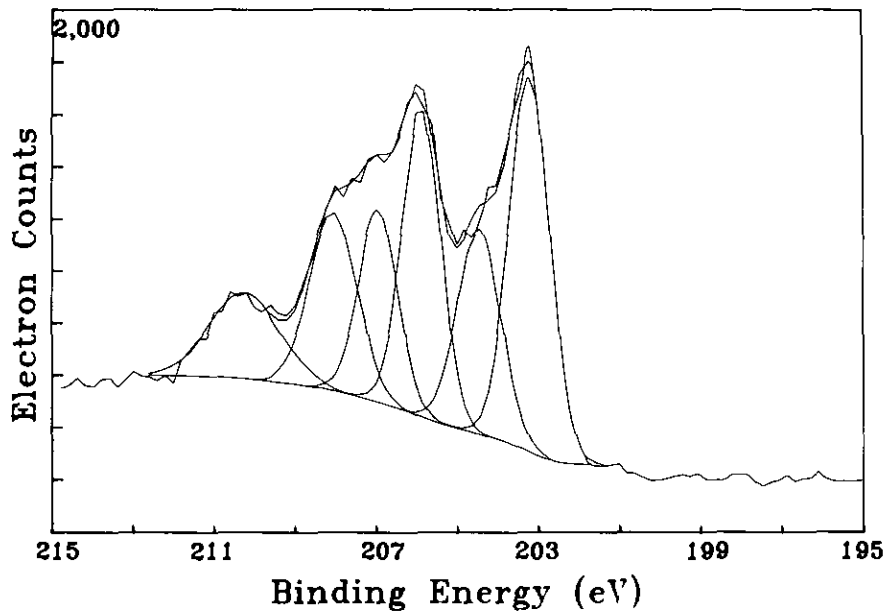

FIG. 4. Nb 3*d* core-level XPS spectrum of $Ba_2Nb_5O_9$. Peaks are sextet and they could be resolved into three pairs of doublets.

Table 3
Niobium $3d_{3/2}$, $3d_{5/2}$ Binding Energy of the $Ba_2Nb_5O_9$ after Argon Ion Sputtering

Binding energy (eV)	State	Intensity (%)
209.2 ± 0.2	$d_{3/2}$ (Nb^{+4})	10
207.0 ± 0.2	$d_{5/2}$ (Nb^{+4})	14
206.0 ± 0.2	$d_{3/2}$ (Nb^{+3})	10
203.6 ± 0.2	$d_{5/2}$ (Nb^{+3})	16
205.0 ± 0.2	$d_{3/2}$ (Nb^{+2})	20
202.2 ± 0.2	$d_{5/2}$ (Nb^{+2})	27

d_{yz}, d_z^2 orbitals are expected to be lowered, and in this circumstance d^2 configuration is stable. There are four oxygen atoms coordinated around Nb(3) and the bond lengths of the two Nb(3)–O(3) and two Nb(3)–O(4) are 2.34 and 2.08 Å, respectively. In this square planar field, the energy levels of d_z^2, d_{xz}, d_{yz} orbitals are expected to be lowered and d^3 configuration is stable.

In $Ba_2Nb_5O_9$, a maximum value of resistivity at 160 K has been observed as reported previously (4). The room temperature resistivity was 6.0×10^{-3} ohm cm with absolute error of 20% and most of the error is due to the uncertainty in the geometry of the electric contacts. We

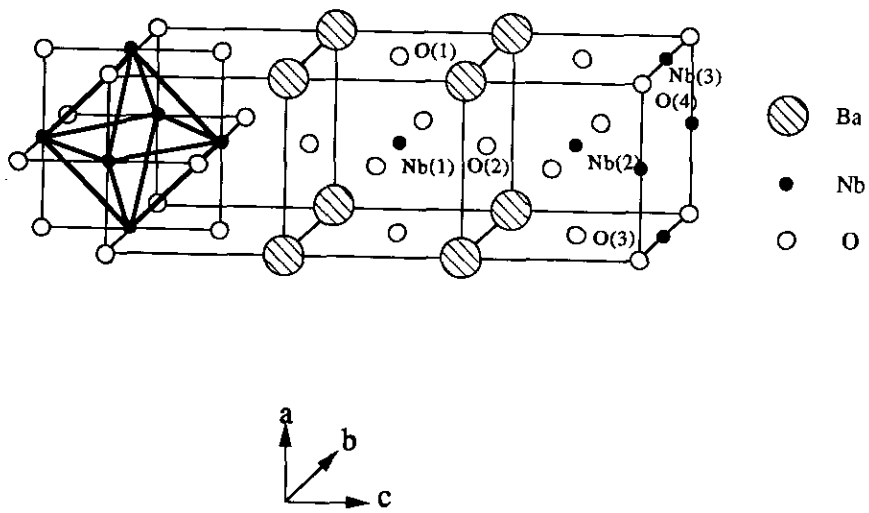

FIG. 5. The structure of $Ba_2Nb_5O_9$. This structure can be described as an alternating building block of perovskite-type NbO_6 layer and Nb_6 octahedra (heavily outlined) layer.

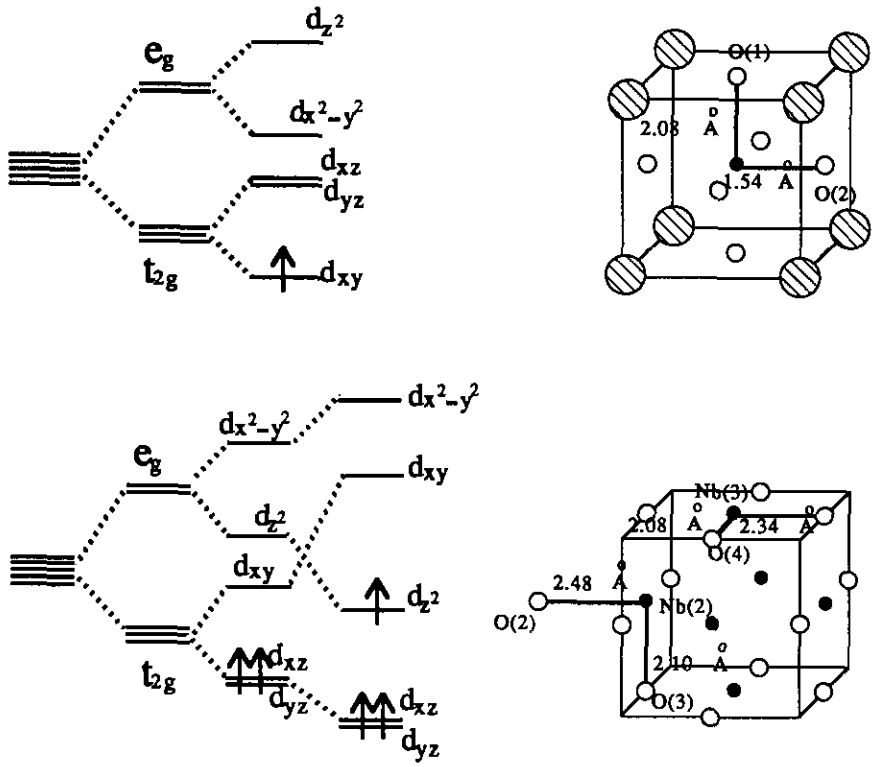

FIG. 6. Splittings of d-orbital energies of (a) in a tetragonally contracted octahedral field (b) tetrahedrally elongated octahedral field and square planar field.

measured the resistivities up to 750 K and found a change in sign of $d\rho/dT$ approximately at 600 K. The $d\rho/dT$ is negative between 160 K and 600 K (Fig. 7). This feature could possibly be driven by a charge density wave (CDW).

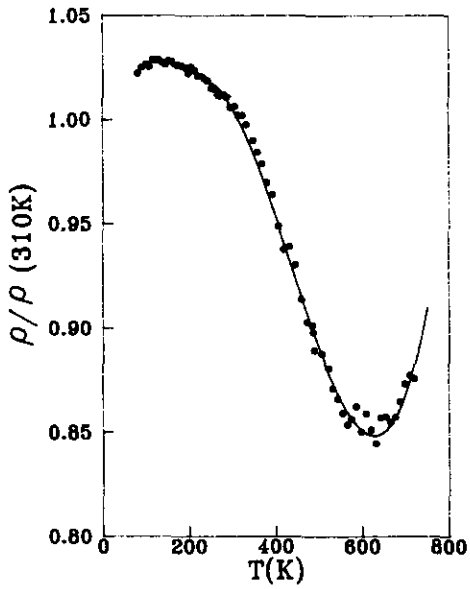

FIG. 7. Normalized resistivity vs. temperature for $Ba_2Nb_5O_9$. A maximum value of resistivity at ~160 K, a change in sign of temperature dependency at ~600 K has been observed.

Similar phenomena are observed for a quasi-one dimensional metallic system such as molybdenium oxide bronze and quasi-low dimensional compounds (12–15). However, no nonohmic behavior was observed for $Ba_2Nb_5O_9$ up to 530 mV/cm in field strength. To examine how the electronic structure is related to physical properties in $Ba_2Nb_5O_9$, we have calculated the electronic band structures of the $Nb_5O_9^{4-}$ unit in $Ba_2Nb_5O_9$ using the parameter in Table 4. The results show the presence of three partially filled d block bands, which indicates the presence of a two-dimensional Fermi surface (Fig. 8). No phase transition at 600 K was confirmed by X-ray diffraction. High-temperature X-ray diffraction (up to 1200 K) patterns did not

TABLE 4
Parameters for EH calculation in $Ba_2Nb_5O_9$

Atom	Orbital	H_{ii} (eV)[a]	$\xi_1(c_1)$	$\xi_2{}^b(c_2)^c$
Nb	5s	−10.10	1.89	
	5p	−6.86	1.85	
	4d	−12.10	4.08(0.6401)	1.64(0.5516)
O	2s	−14.8	2.275	
	2p	−33.3	2.275	

[a] H_{ii}, valence orbital ionization potential.
[b] ξ, Slater-type orbital exponents.
[c] c, coefficients used in double-ξ expansion of orbitals.

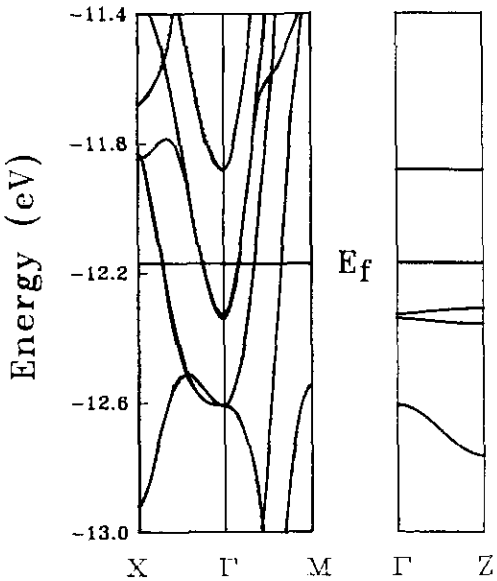

FIG. 8. Low-lying d-block bands calculated for the Nb_5O_9 unit in $Ba_2Nb_5O_9$. The results show the presence of three partially filled d-block band which indicates open Fermi surface along ab layer direction.

have any difference from those at room temperature. This result suggests that the change in sign of $d\rho/dT$ at 160 and 600 K is not due to structural phase transition or any thermal disintegration.

To further examine the anomalous electronic behavior, $Ba_{2-x}Y_xNb_5O_9$ ($x = 0.05, 0.10, 0.20$) were prepared. When x increased, the cell parameters decreased as shown in Fig. 9. The Raman spectra of these compounds confirm that the yttrium dopants substituted Ba sites. As shown in Table 5 six peaks in total were observed in various compositions of $Ba_{2-x}Y_xNb_5O_9$. Because the space group of this compound is $P4/mmm$, A_{1g}, B_{1g}, and E_g modes are expected to be observed. Figure 10 shows the modes

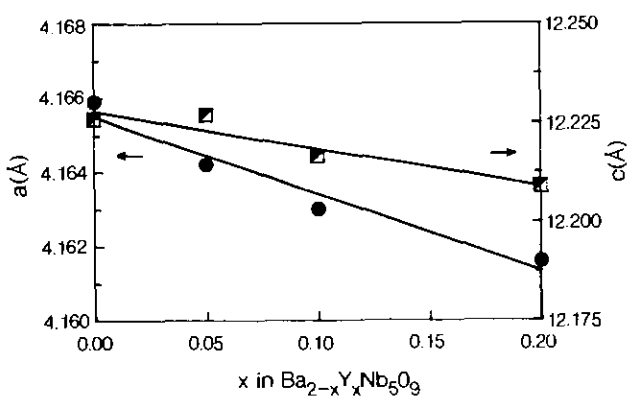

FIG. 9. Change in the lattice parameters a and c as a function of Y content in $Ba_{2-x}U_xNb_5O_9$.

TABLE 5
Frequencies in cm^{-1} of Raman vibrational modes in $Ba_{2-x}Y_xNb_5O_9$

	Raman shift (cm^{-1})					
Composition (x)	ν_1	ν_2	ν_3	ν_4	ν_5	ν_6
0	131	162	237	503	539	634
0.05	135	162	236	503	536	629
0.1	136	161	237	503	538	633
0.2	139	163	237	502	537	630

at low frequencies along with an Ar-plasma line at 117 cm^{-1}. Among 6 peaks, only the peak with lowest frequency, 131 cm^{-1}, shifted to higher frequency when the yttrium content increased. The increase of the frequency of Ba A_{1g} mode suggests that the lighter yttrium atoms substituted for Ba atoms.

For $Ba_{2-x}Y_xNb_5O_9$ samples as well, negative $d\rho/dT$ behavior was observed, but the maxima of resistivity were observed at a higher temperature than in the undoped sample. Resistivity curves normalized to 1 at 297 K are shown in Fig. 11 along with that of undoped sample. All yttrium-doped samples show negative $d\rho/dt$ behavior above 230 K, which is at a higher temperature than in the undoped sample. The positive $d\rho/dT$ behavior is usually regarded as metallic and the negative $d\rho/dT$ behavior as semiconducting. However, even if it is not metallic the positive $d\rho/dT$ behavior is also possible from the tempera-

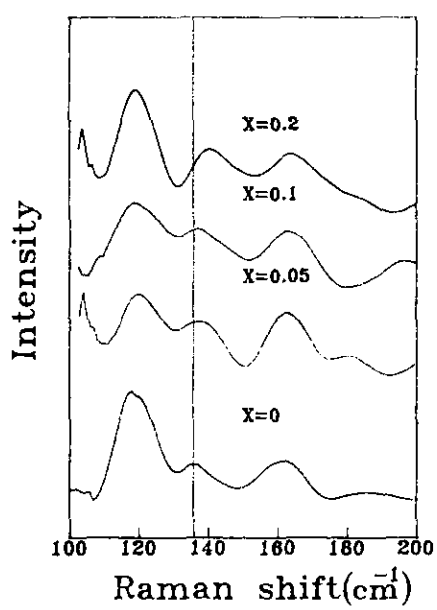

FIG. 10. Raman spectra of $Y_xBa_{2-x}Nb_5O_9$ ($x = 0.00, 0.05, 0.10, 0.20$). The peak near 117 cm^{-1} is a Ar-plasma line. Note the shift of 131 cm^{-1} mode with Y substitution on Ba site.

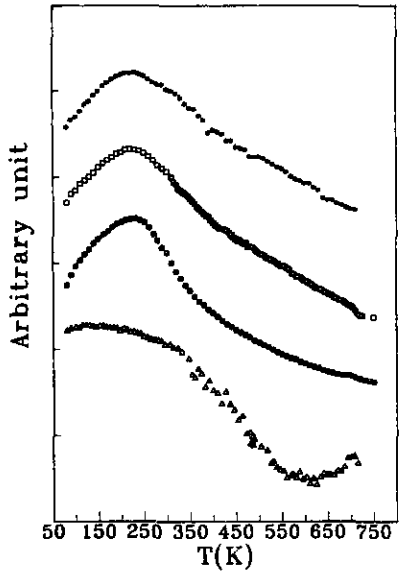

FIG. 11. Normalized resistivity vs temperature for $Y_xBa_{2-x}Nb_5O_9$ (x = 0.00, 0.05, 0.10, 0.20 from bottom to top). Resistivity is plotted on a linear scale

ture dependence of the in-plane lifetime of the carriers which tunnel to the neighboring planes in two-dimensional metals (16). In such a case, the $d\rho/dT < 0$ behavior may come from phonon-assisted hopping when disorder is introduced between the planes (8). However, our samples are polycrystalline. Thus, the resistivity curves represent a mixture of in-plane and interplane resistivities. For the undoped sample ($x = 0$), in-plane resistivity seems to be small, thereby leading to a smooth temperature-dependence of resistivity. As the samples are doped by yttrium, the disorder effect seems to increase the in-plane resistivity. This would make the total resistivity more strongly determined by the interplane resistivity, which has a $d\rho/dT < 0$ behavior at high temperature due to phonon-assisted hoping as disorder sets in. The three curves ($x = 0.05, 0.10, 0.20$) show a maximum at almost identical temperatures. It is possible that the substitution of Y is saturated by the amount of $x = 0.05$.

Michelson *et al.* reported electrical resistivity of single phase $BaSrNb_5O_9$ with lattice constants $a = 4.150$ Å, $c = 12.021$ Å (4). In the measured temperature range below 325 K, the resistivity does not show any maximum as does $Ba_{2-x}Y_xNb_5O_9$. In $BaSrNb_5O_9$, which has much smaller lattice parameters than $Ba_{2-x}Y_xNb_5O_9$, the in-plane lifetime of the carriers would be much shorter than in $Ba_{2-x}Y_xNb_5O_9$ due to more active hopping. Therefore the total resistivity, which is determined by the competition between the in-plane lifetime term and the phonon-assisted term, is expected to show its maximum at much higher temperatures than 230 K, possibly higher than 325 K. Obviously, it is not ruled out that the $d\rho/dT < 0$ behavior could come from the semiconducting nature or even from the decrease of the c-axis band gap with increasing temperature.

In summary, we prepared two reduced niobates, $BaNbO_3$ and $Ba_{2-x}Y_xNb_5O_9$. Raman results in $Ba_{2-x}Y_xNb_5O_9$ confirm that Y atoms substitute in Ba sites. XPS experiments indicate that there are three different oxidation states of niobium in $Ba_2Nb_5O_9$ and one oxidation state of Nb^{4+} in $BaNbO_3$. Based on electrical resistivity measurements, we suggest that the negative resistivity versus temperature dependence originates from phonon-assisted hopping between planes as disorder is introduced.

ACKNOWLEDGMENTS

The present studies were supported by the Korean Ministry of Education Research Fund for Advanced Materials 1991–1992 and in part by Korean Science and Engineering Foundation (92-25-00-02). We thank Dr. H. F. Franzen (Iowa State University) for his help in high temperature X-ray diffraction studies. Thanks are also due to Dr. Y-M. Kim in KIST for helping with the XPS experiments. We thank Dr. W. Kang (Ewha Women's University) for his helpful discussions and suggestions.

REFERENCES

1. G. Svensson, *Mater. Res. Bull.* **23,** 437 (1988).
2. G. Svensson, *Acta Chem. Scand.* **44,** 222 (1990).
3. G. Svensson, J. Köhler, and A. Simon, *Acta Chem. Scand.* **46,** 244 (1992).
4. C. E. Michelson, P. E. Rauch, and F. J. DiSalvo, *Mater. Res. Bull.* **25,** 971 (1990).
5. D. Ridgley and R. Ward, *J. Am. Chem. Soc.* **77,** 6132 (1955).
6. R. Kreiser and R. Ward, *J. Solid State Chem.* **1,** 368 (1970).
7. G. Svensson, *Mater. Res. Bull.* **25,** 9 (1990).
8. L. Forro, V. Hakovac, J. R. Copper, C. Ayache, and J.-Y. Henry, *Phys. Rev.* **B 46,** 6626 (1992).
9. A. Sakthivel and R. A. Young, "Program DBW9006PC for Rietveld Analysis of X-ray and Neutron Powder Diffraction Patterns." 1990.
10. R. Hoffmann, *J. Chem. Phys.* **39,** 1397 (1963).
11. National Institute of Standards and Technology, "XPS Standard File."
12. M. Greenblatt, *Chem. Rev.* **88,** 31 (1988).
13. E. Canadell and M. H. Whangbo, *Chem. Rev.* **91,** 965 (1991).
14. E. Wang, M. Greenblatt, I. E. Rachidi, E. Canadell, and M. H. Whangbo, *Inorg. Chem.* **28,** 2451 (1989).
15. M. H. Whangbo and L. F. Schneemeyer, *Inorg. Chem.* **25,** 2424 (1986).
16. G. Soda, D. Jerome, M. Wegar, J. Alizon, J. Gallice, M. Robert, J. W. Fabre, and G. Giral, *J. Phys. Paris* **38,** 931 (1977).